Design, Manufacturing and Implementation of a Novel 2-Axis Force Sensor for Haptic Applications.

A. Buttafuoco[a,1,*], C. Lenders[a,2], R. Clavel[b,3], P. Lambert[a,2], M. Kinnaert[a,1]

[a] *Université Libre de Bruxelles, Av. F.D. Roosevelt 50, CP165, 1050 Bruxelles, Belgium*
[b] *EPFL STI IMT LSRO2 ME B3 426, Station 9, CH-1015 Lausanne*

Abstract

Minimally invasive surgeries on the lungs have eliminated the ability for surgeons to place their hands on the patient's organ to feel for abnormalities. Therefore, in this paper, a force sensor for 2 degrees of freedom haptic applications is described. Its integration within a force feedback teleoperated device would allow the medical doctor to essentially feel the lung without making physical contact. Its design relies on a specific elastic frame. The latter is based on two flexible structures bending around the same axis, in order to reduce cross-sensitivity. The manufacturing by wire electrical discharge machining allowed to obtain a monolithic, compact and highly precise structure.

The force sensor has been sized on the basis of the study of the flexible parts it is made of. Next, it has been characterized and implemented on an haptic interface reproducing the contact with a human lung. The results show that the developed sensor is adequate to the study of lung palpation.

Keywords: force sensor; compliant mechanism; haptic application; lung; medical device

[*]Corresponding author

Email addresses: `angelo.buttafuoco@ulb.ac.be` (A. Buttafuoco), `cyrille.lenders@ulb.ac.be` (C. Lenders), `reymond.clavel@epfl.ch` (R. Clavel), `pierre.lambert@ulb.ac.be` (P. Lambert), `michel.kinnaert@ulb.ac.be` (M. Kinnaert)

[1]Control Engineering and System Analysis Dpt, Université Libre de Bruxelles
[2]Bio, Electro and Mechanical Systems Dpt, Université Libre de Bruxelles
[3]Laboratory of Robotic Systems, Swiss Federal Institute of Technology Lausanne

1. Introduction

The force sensor described in this paper has been designed in the framework of a proof of concept for a force-feedback teleoperated palpation tool adapted to minimally invasive thoracic surgery.

Minimally invasive surgery (MIS) consists in operating through small incisions in which a camera and adapted instruments are inserted. It allows to perform many interventions with reduced trauma for the patient. One of these is the ablation of peripheral pulmonary nodules.

Nevertheless, the means for detecting nodules during MIS are limited. In fact, because of the lack of direct contact, the surgeon cannot palpate the lung to find invisible lesions, as he would do in classical open surgery. As a result, only clearly visible nodules can be treated by MIS presently.

A suitable solution to this problem consists in using a teleoperated palpation instrument, in order to extend the possibilities of MIS in the thoracic field. Such an instrument is made of a master device, manipulated by an operator, and a slave device which is in contact with the patient and reproduces the task imposed by the master. Adequate control laws between these two parts allow to restore the operator's haptic sensation (Hokayem [1]).

Such a device is being developed in our team. Its goal is to provide kinesthetic force feedback, i.e. to restore the information of contact coming from the muscles and joints.

At the present time, the master of the device, a planar pantograph-like mechanism, is used as a haptic interface reproducing the contact with a human lung. It can be used to study palpation or to train surgeons. A 2-axis force sensor is therefore required to equip this haptic interface. Later, this force information will be used to implement advanced teleoperation control schemes.

The study of haptics often involves 2 degrees of freedom (dof) devices (Campion et al. [2], Spaelter et al. [3], Smith et al. [4]). Force measurements along these 2 axis are useful for several reasons. They may be used within control loops to improve the user's comfort and security. In addition, they allow to compare the expected interaction force between the user and the device to the actual one for validation purposes, or to study the force involved in a particular gesture.

Conventional commercial force sensors are usually inadequate for 2 dof haptic applications : most of them are very expensive and provide 6-component measurements, while the more affordable 2- and 3-axis force sensors are bulky

and account for much wider ranges than the one required. These observations usually lead researchers to develop their own force sensors for their specific applications (Spaelter et al. [3], Tada et al. [5], Chen and A. [6], Ki [7]). Most of the time, they are made of the serial concatenation of flexible structures, each one bending easily around only one axis. The measurement of the structure displacement is related to the force in that direction. However, this results in sensors with cross-sensitivity of a few percents.

A fraction of this cross-sensitivity can be attributed to the design of the sensors. Each flexible part of these sensors is supposed to bend along one axis. Nevertheless, when a force is applied on the sensor, a displacement occurs in all the parts, due to the finite stiffness of the matter. This results in a parasitic strain, that can be interpreted as a force along an unsolicited axis.

This phenomenon can be an issue if the forces to measure along two different axes have a different order of magnitude. To avoid this problem, the 2 dof force sensor presented in this paper is made of 2 flexible structures working in parallel, and bending in the same direction. The force along each axis is reconstructed from the combination of the displacement of both structures. The resulting sensor is monolithic, compact and low-cost. Moreover, it has a very linear behavior and a good precision.

The developed force sensor has been implemented on a 2 dof haptic interface reproducing the contact with a human lung. The considered model of the lung embeds a pulmonary nodule. The haptic interface has been validated by an experienced thoracic surgeon. Therefore, it can be used to study the lung palpation or to train surgeons to perform the latter gesture.

The paper is organized as follows. The elastic frame is presented in Sec.2, where its operating principle and some general elements of sizing are discussed. Then, the implementation of the sensor on the haptic interface is detailed in Sec. 3. The latter section successively addresses the sizing of the sensor for the application at hand, the characterization of this sensor and the presentation of the results of the palpation experiment. Finally, we sketch the medical tool embedding the current and future developments. The conclusions are presented in Sec. 4.

2. The Elastic Frame of the Force Sensor

2.1. Operating Principle

The elastic frame is based on the statically determinate beam represented in Fig. 1 . Let F_x and F_y be the forces applied along the x and y axes respectively, and N_A, N_B and N_x, the reaction forces. The equilibrium equations of the system are :

$$N_A + N_B = F_y$$
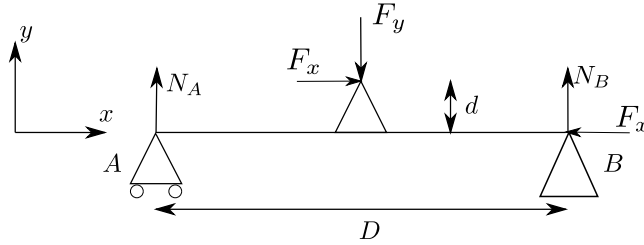
$$N_B D = F_y \frac{D}{2} + F_x d \tag{1}$$

Figure 1: Statically determinate beam of length D. F_x and F_y are respectively the forces along the x and y axes, applied on a pin support of height d. N_A and N_B are the vertical reaction forces respectively at the roller support A and the pin support B.

As can be seen in Eq. (1) , the forces F_x and F_y can be computed on the basis of the knowledge of the reaction forces N_A and N_B. Since these reaction forces are both vertical, they can be measured using two springs with a known stiffness placed under the supports A and B. The deflection of each spring is then proportional to the respective reaction force.

This idea has been exploited for the design of the elastic frame shown in Fig. 2.

In fact, the blade noted A cannot resist horizontal forces without bending. On the other hand, vertical efforts can be held with only a very small deformation of the blade in that direction. In that sense, the blade A behaves like a roller support. The compliant pivot B is made of 2 perpendicular blades. It can withstand both horizontal and vertical efforts, but allows for the rotation around their intersection point. The forces applied on A and
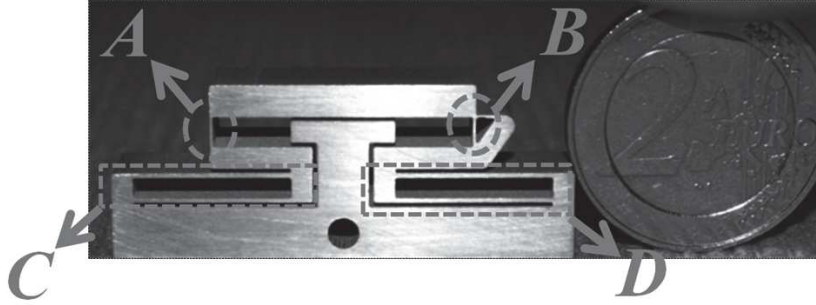
4

Figure 2: Elastic frame made of a flexible rolling support (A), a flexible pivot (B) and 2 flexible springs (C and D).

B are transmitted to the plate-springs C and D. As the motion of these 2 elements is constrained by 2 parallel blades, their extremity will translate almost vertically. Thus, the forces applied on the top of the elastic frame are related to the deformation of C and D. Compression forces make the plate-springs move in the same direction with the same amplitude, while the torque induced by horizontal forces makes the plate-springs move in opposite directions with the same amplitude. This phenomenon is used to discriminate vertical and horizontal forces.

2.2. Elements of Sizing

2.2.1. General Hypotheses

The modeling of flexible structures is based on the following assumptions :

- The matter is homogeneous, isotropic and continuous. This hypothesis is generally verified.

- Only small deformations in the elastic domain are considered and Hooke's law applies, i.e. the strain is proportional to the stress. This law can be written as follows :
$$\sigma = E\epsilon \tag{2}$$
with σ, the stress applied on the structure, E the Young's modulus and ϵ the resulting strain.

- The curvature $\frac{1}{\rho}$ of a beam is approximately equal to the second derivative of its deflection, i.e. if the shear is negligible compared to the

5

bending :

$$y(x)'' \simeq \frac{1}{\rho} \simeq \frac{M(x)}{EI(x)} \qquad (3)$$

where x is the abscissa of the considered section of the beam, y is the ordinate of the neutral fiber, M is the bending moment and I is the second moment of area of the section at hand, according to Fig.3. This equation usually provides an excellent approximation.

A study of the parallel-guided plate-springs based on these hypotheses is presented in the next subsection. More information can be found in (Henein [8]).

2.2.2. Sizing of the Parallel-Guided Plate-Springs

On the basis of the description in Sec. 2.1, it is clear that the precision of the force measurement depends on the sizing of the plate-springs C and D. Indeed, Parts A and B only make the structure statically determinate. Thus, their sizing has to guarantee that they will behave respectively as a roller support and a pivot. Let us first address this issue before dealing with the plate-springs. The required behavior for parts A and B is ensured provided the following two conditions are fulfilled.

First, the blades composing parts A and B have to be slender enough, i.e. their length l, width b, and thickness h, as defined in Fig.3 , must satisfy the following relations (Henein [8]) :

$$10h \leq l \; ; \; 10h \leq b \qquad (4)$$

Second, the stress σ applied on the elements A and B has to stay under an admissible limit σ_{adm} to make sure the deformation remains within the elastic domain :

$$\sigma < \sigma_{\mathrm{adm}} < \sigma_{\mathrm{yield}} \qquad (5)$$

with σ_{yield}, the yield strength of the considered material.

Let us now present the laws that will be used for the sizing of the plate-springs C and D for our specific application in Sec.3.2. The vertical deformation of these springs is used as a measure of the applied force. Its range depends on the spring stiffness and directly influences the sensor sensitivity. Expressions for these quantities are provided next.
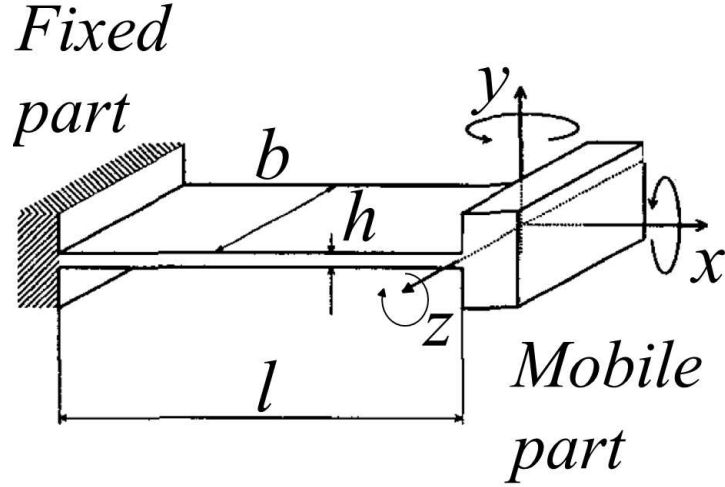
Figure 3: Flexible blade of length l, width b and thickness h. Adapted from (Henein [8])

Elements C and D are both made of two parallel identical flexible blades sized in order to fulfil conditions (4) and (5). A representation is given in Fig.4. An in-depth study of these structures can be found in (Henein [8]).

When the transverse load $\bar{N}$ represented in Fig.4 is null, the force $\bar{P}$ causes the displacement f and the two blades act in parallel, so that the no-load translational stiffness of their assembly is given by $\bar{K}_0$:

$$\bar{K}_0 = \frac{\bar{P}}{f} = \frac{24EI}{l^3} = 2K \tag{6}$$

with E, the Young's modulus of the material, $I = \frac{bh^3}{12}$, the second moment of area of a single blade and $K = \frac{12EI}{l^3}$, the translational stiffness of a single blade.

However, in the configuration of the elastic frame depicted in Fig.2, the springs are loaded transversally. Indeed, both a vertical and a horizontal force can be applied on the top of the device and transmitted to the plate-springs. Considering that a load $\bar{N} \neq 0$ is applied between the two blades of the spring, the translational stiffness of the loaded spring, noted $\bar{K}$, has to be corrected in the following way :
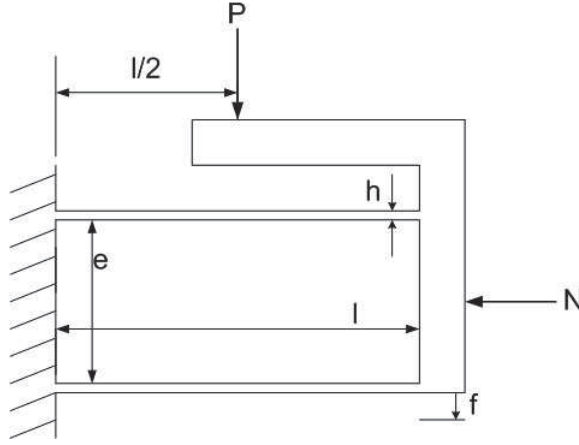
Figure 4: Translational spring made of the assembly of 2 flexible blades, adapted from (Henein [8])

$$\bar{K} = \frac{\bar{P}}{f} \simeq \bar{K}_0(1 - \frac{\bar{N}}{\bar{N}_0}) \qquad (7)$$

where $\bar{N}_0 = \frac{\pi^2 EI}{l^2}$ is the axial load that cancels the stiffness of the spring. When knowing the maximal transverse load, an adequate sizing of the spring allows to make $\frac{\bar{N}}{N_0} \ll 1$, so that relation (6) still holds.

The relation between the admissible displacement f_{adm} and the admissible stress σ_{adm} can be expressed as follows :

$$f_{\text{adm}} = \frac{\sigma_{\text{adm}} l^2}{3Eh} \qquad (8)$$

It is to note that unless $\bar{P}$ is applied in the middle of the flexible blades, the induced torque causes one of the blade to elongate and the other to contract. This result in a shifting of the mobile part, and consequently, its motion will stop being purely translational.

On the basis of these equations, the sizing and the implementation of the force sensor on a medical haptic application is detailed in the next section.

3. Implementation of the Force Sensor

As mentioned in the introduction, the force sensor described in this paper has been designed in the framework of a proof of concept for a force-feedback

teleoperated palpation tool adapted to minimally invasive thoracic surgery. Its goal is to provide kinesthetic force feedback, i.e. to restore the information of contact coming from the muscles and joints.

At the present time, the master of the device, a planar pantograph-like mechanism, is used as a haptic interface reproducing the contact with a human lung. It can be used to study palpation or to train surgeons. A 2-axis force sensor is therefore required to equip this haptic interface. Later, this force information will be used to implement advanced teleoperation control schemes.

3.1. Description of the Haptic Interface

3.1.1. Mechanical device

The haptic interface is represented in Fig.5. The useful workspace is delimited by a plastic border. The links of the device are sized to maximize the manipulability in that zone, while minimizing the required torques, the bulk and the weight.

The motor torques are increased thanks to capstan systems instead of gearboxes, to avoid backlash and to keep the friction low. The position of the lower arms of the device is measured with 512 cpt encoders.

The force sensor is mounted on an axis at the top of the device. A double-parallelogram system keeps its orientation horizontal. The handle is a roller bearing fixed to the top of the force sensor. It avoids the operator to apply a torque that could interfere with the horizontal force measurement.
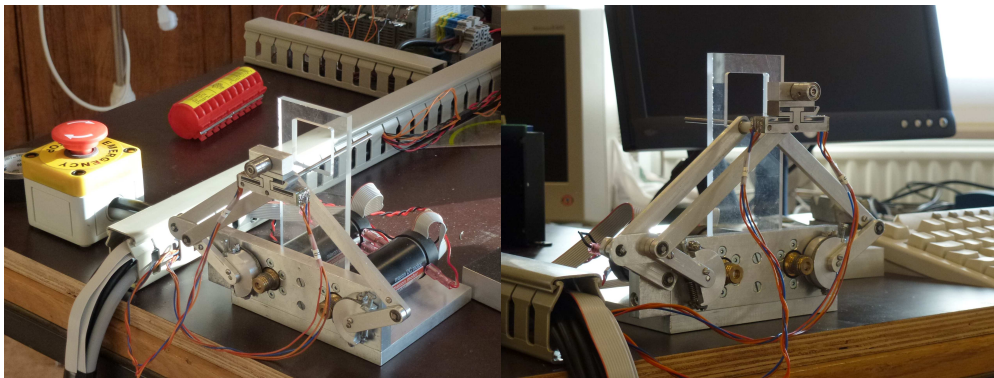

Figure 5: Force sensor mounted on the haptic interface.

3.1.2. Lung Model

The model of the lung developed for the haptic interface is detailed in (Nicotra et al. [9]). It consists of a hybrid model that reproduces the viscoelastic behavior of the lung using standard linear solids.

To avoid the issues related to ex-vivo experiments, the viscoelastic parameters of the lung have been identified on a gel mock-up, built in collaboration with thoracic surgeons in a previous work.

Two modes are taken into account in the hybrid model, depending on the situation:

- A contact mode, where the operator is in contact with the surface of the lung. In this case, the surface deforms, and the horizontal and vertical components of the reaction force of the virtual lung are computed on the basis of the operator's position and velocity.

- A non contact mode, where the operator moves above the surface of the lung. Then, the lung relaxes until its surface reaches its initial position or the operator's position.

According to the mode and to the Cartesian position and velocity of the operator's finger, the vertical and horizontal reaction forces of the lung are computed, and converted to joint torques using the kinematics of the mechanical device.

In addition to that model, a pulmonary nodule is modeled as a stiff ball attached to a spring. This allows the virtual nodule to move just like a real one fixed to a bronchiole or a small artery. The oedema around the lesion has also been reproduced in the virtual reality as a zone of higher stiffness in the neighborhood of the lesion.

3.1.3. Specifications for the Force Sensor

Basically, the force sensor will be used to measure the compression and the shear forces applied by the operator during palpation. These two forces have different magnitudes. On the basis of previous experiments, the range of the sensor has to reach $10\,\mathrm{N}$ in compression, and $2\,\mathrm{N}$ in shear.

In addition, the sensor has to be rigid enough not to influence the operator's behavior. A stiffness of several tens of $\mathrm{kN\,m^{-1}}$ is generally required.

Moreover, a cut-off frequency of $300\,\mathrm{Hz}$ is considered as good practice for control purposes.

Finally, the size and bulk of the sensor have to permit an easy implementation on the master device.

Note that, at this stage, sterilizability issues are not taken into account.

3.2. Sizing and Manufacturing of the Force Sensor

A 1060 aluminum alloy has been chosen to build the sensor. It has a Young's modulus E equal to $69\,\mathrm{GPa}$ and its yield strength σ_{yield} is $400\,\mathrm{MPa}$. The admissible stress σ_{adm} is limited to $200\,\mathrm{MPa}$ to avoid plastic deformations.

Strain gauges are used to measure the plate-spring deflections, due to their low cost and ease of use. Each of the plate-springs C and D has been sized to have a no-load translation stiffness of about $25\,\mathrm{kN\,m^{-1}}$, computed with (6). A length of $15\,\mathrm{mm}$ and a width of $10\,\mathrm{mm}$ have been chosen for each of the blades they are made of, to make the bonding of the gauges easier. With a thickness of $0.4\,\mathrm{mm}$, this leads to a stiffness of $26.17\,\mathrm{kN\,m^{-1}}$ for each spring. As the latter are mounted in parallel, the theoretical overall stiffness of the sensor K_{tot} is $52.34\,\mathrm{kN\,m^{-1}}$.

To avoid the shifting of the top of the sensor, parts A and B have been placed to transmit the forces just in the middle of the springs C and D, respectively.

As the maximal shear force applied by the operator on the lung is known and equal to $2\,\mathrm{N}$, the absolute value of the largest transverse load $\bar{N}$ applied on each plate-spring is $1\,\mathrm{N}$. Thus, the ratio $\frac{\bar{N}}{N_0}$ will not exceed 0.0061, and according to (7), the following expression is valid :

$$K_{\mathrm{tot}} \simeq 2\bar{K}_0 \tag{9}$$

so that the stiffness of the sensor can be considered as independent of the transverse load.

The admissible displacement f_{adm} of the mobile part computed with (8) is equal to $0.54\,\mathrm{mm}$. For security purposes, stops prevent the mobile part from exceeding a displacement of $0.5\,\mathrm{mm}$.

Regarding compactness, the external size of the sensor is only $20 \times 36 \times 10\,\mathrm{mm^3}$. The total mass is $12\,\mathrm{g}$, and the mobile part of the sensor has a mass, noted m_{mp} of $4\,\mathrm{g}$. Since the first eigenfrequency of the sensor is an indicator of its cut-off frequency, the latter can be estimated by $\frac{1}{2\pi}\sqrt{\frac{K_{\mathrm{tot}}}{m_{\mathrm{mp}}}} = 573\,\mathrm{Hz}$, which is above the $300\,\mathrm{Hz}$ specified bandwidth.

Based on these results, the elastic frame has been manufactured using electrical discharge machining leading to a compact and monolithic structure. Experiments have allowed to estimate the actual stiffness of the elastic frame, which is $42\,\mathrm{kN\,m^{-1}}$. The difference between the theoretical and the actual stiffness can be mostly attributed to manufacturing tolerances of the translational springs. Indeed, by injecting $I = \frac{bh^3}{12}$ in (6), it can be seen that even a minor variation in thickness with respect to the nominal value can induce a significant difference in the expected stiffness of the spring.

The cut-off frequency computed on the basis of the actual stiffness of the sensor is $3240\,\mathrm{Hz}$. However, the bandwidth of the force signal is limited to $500\,\mathrm{Hz}$ by the amplifiers, as explained below. Yet, this is sufficient for control purposes. After proper sizing of the sensor, its experimental characterization is reported in the next section.

3.3. Characterization of the Force Sensor

Strain gauges have been bonded on the surface of the plate-springs, next to their fixed part, and quarter Wheatstone bridges have been implemented. Let V_C and V_D be the outputs of the Wheatstone-bridge attached respectively to the plate-spring C and D in Fig.2. On the basis of the behaviour described in Sec.2.1, the horizontal and vertical forces can respectively be related to the tensions V_t and V_f computed as follows :

$$
\begin{aligned}
V_\mathrm{f} &= V_C + V_D \\
V_\mathrm{t} &= V_C - V_D
\end{aligned}
\tag{10}
$$

Amplifiers with a $500\,\mathrm{Hz}$ bandwidth have been connected to each strain gauge circuit to condition the signal. The strain gauge circuits have been powered with $5\,\mathrm{V}$, and the amplification factor is 500.

To establish the relation between the output of the sensor circuit and the applied force, the sensor has been fixed to a rotation axis. A bolt has been attached at the top of the sensor. Known weights have been fixed on it thanks to a nut.

The sensor has been rotated by steps of $30°$ until its complete revolution was achieved. The tensions V_t and V_f have been computed for each position on the basis of the measurements of V_C and V_D. This procedure has been re-iterated four times with each weight, alternating clockwise and anti-clockwise rotations. The following weights have been used : $1\,\mathrm{g}$, $105\,\mathrm{g}$, $210\,\mathrm{g}$ and $315\,\mathrm{g}$.
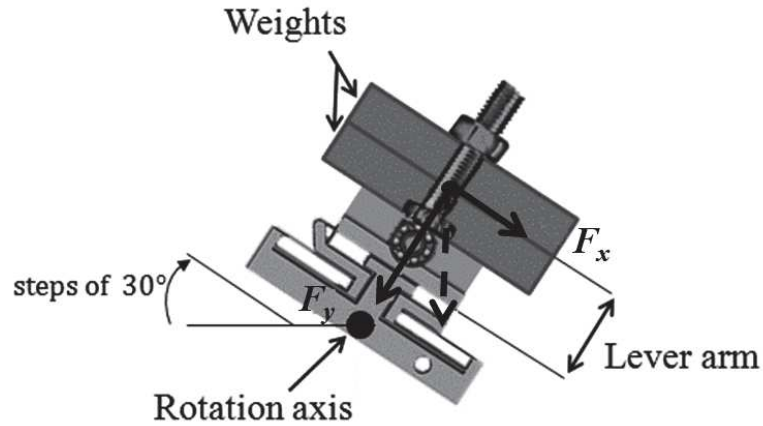
Figure 6: Characterization of the force sensor. Known weights are attached to the top of the device thanks to a bolt and nut system. The device is then rotated by steps of 30°. V_t and V_f are computed in each position on the basis of the voltage output of the Wheatstone bridges.

By means of the rotation, they allow to test many combinations of forces along the 2 axes of the sensor.

As the height of the weights increases, so does the lever arm between the load and the plate-springs, as illustrated in Fig.6. The values of the forces applied on the top of the sensor are reported to equivalent forces applied on the sensor handle in Fig.7.

Due to the increasing lever arm, the force along the shear axis is not of the same order of magnitude as the force along the compression axis. In order to reach 10 N along the compression axis with no saturation along the shear axis, a second experiment has been carried out inducing compression force only. Weights of 205 g, 210 g, 238 g, 258 g and 268 g have been successively added on the top of the sensor in order to reach about 10 N, then removed one at a time. Three charge-discharge cycles have been performed in a row, without resetting the zero.

Figure 7 shows the data collected during the whole characterization protocol. As one can see, the sensor is very linear, and provides high repeatability and low hysteresis.
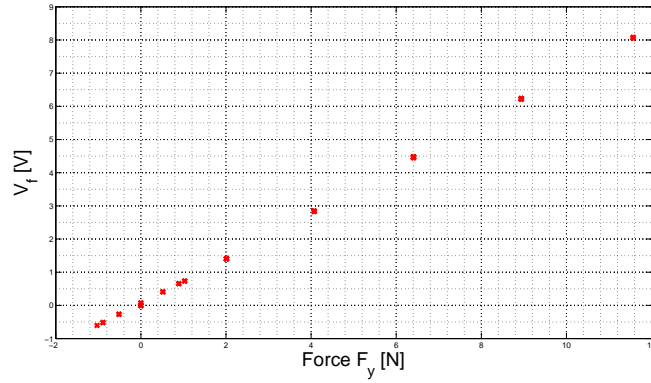
The law of the sensor identified by a least squares method based on this set of data is the following :

13

$$\begin{aligned}
F_x &= 0.62[\text{N V}^{-1}]V_\text{f} + 0.06[\text{N}] \\
F_y &= 1.53[\text{N V}^{-1}]V_\text{t} - 0.08[\text{N}]
\end{aligned} \qquad (11)$$

with F_x the shear force and F_y the compression force.
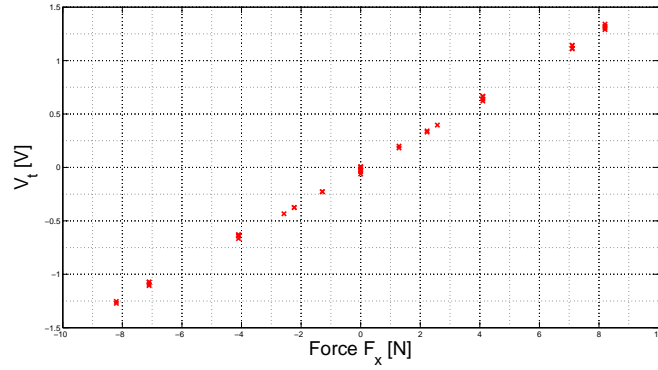
(a) Relation between F_x and V_t

(b) Relation between F_y and V_f

Figure 7: Characterization of the force sensor

The overall precision of the sensor is 3.2% of the rated output for the measure of F_x and 1.5% for the measure of F_y.

Now that the sensor has been characterized, let us return to the considered application.

3.4. Palpation Experiment

A palpation experiment has been carried out on the haptic interface. The goal was to understand the kind of force information associated with the discovery of a nodule by the operator. The operator was asked to search the area within the plastic frame of the haptic interface (see Fig. 5) in order to discover a hidden nodule of 1 cm diameter. It is to note that he had no medical experience, but was familiar with the concept of haptic interface.

The strategy adopted by the operator consisted in pressing the virtual lung vertically in several spots until he suspected the presence of a nodule. On that spot, horizontal back and forth have been performed. The measured forces are reported in Fig. 8.

The first two time intervals (up to 9 s) correspond to the first vertical probings. The horizontal force F_x measured during these time intervals is the one needed to move the device to another location. During the third time interval, back and forth movements are performed in order to move the nodule horizontally.

As one can see, a characteristic force profile appears in the compression force F_y each time the operator passes on the nodule. As the nodule is moved away by the horizontal motion, the vertical stiffness of the virtual lung suddenly drops. This information can be exploited for the development of the teleoperated device. Indeed, those patterns can be detected and amplified in order to make the localization of a very small nodule easier.

Given the design of the haptic interface, a possible torsional effect due to the positioning of the handle (see Fig. 5) might affect the measured forces. This issue is addressed in the following remark.

Remark on Torsion

As shown in Fig.5, the haptic interface is manipulated through a handle, attached to the force sensor. Due to the length of this handle, some torsion may appear in the plate-spring, as compression forces are applied.

The stiffness of the structure with respect to torsion has been investigated on the CAD model of the sensor using a finite elements method, as shown in Fig.9. The idea is to compare the effect of bending and torsion on the elongation of the strain gauges when the maximaum expected torque is applied, i.e. when a $10\,\text{N}$ vertical force is applied through the $1\,\text{cm}$ long
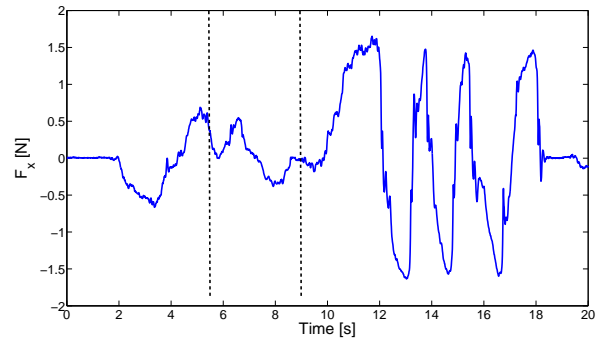
(a)
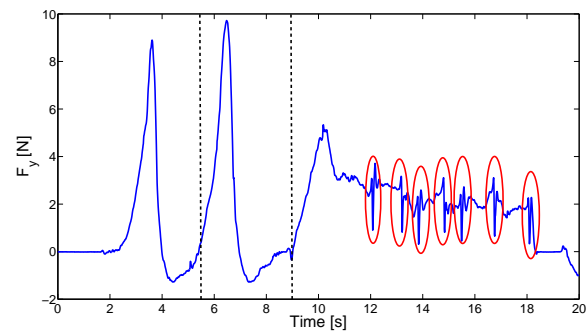
(b)

Figure 8: Force measurements during a palpation experiment on the haptic interface. The force pattern associated with the lateral motion of a nodule is highlighted by ellipses.

16

handle attached to the force sensor. The results show that the elongation and compression stresses due to torsion on the strain gauges are 2 orders of magnitude smaller than the elongation stress due to bending. Moreover, they are practically symmetric with respect to the median plane of the elastic frame. As a consequence, for a torsion around the $x-$axis, the effect of the compression on the Wheatstone bridge will be approximately compensated by the effect of the elongation. Thus, the measured parasitic force caused by the maximal expected torsion can be neglected when compared to the total force measurement.

3.5. Presentation of the Targeted Medical Tool

The haptic device used for the palpation experiment is actually the master of a teleoperated palpation tool presently developed within our team. A scheme of the tool is represented in Fig.10. The pantograph-like master is supported by the operator with one hand and manipulated with his other thanks to the handle at the top of the device. Horizontal and vertical displacements can be performed. The forces in these directions are measured by the force sensor mounted on the top of the device.

The slave grasper is the part intended to enter the patient's body. It has 2 moving arms. The upper one acts in compression, the lower one in shear. The opening and closure of the upper arm is commanded by vertical displacements of the master, while the shear movements are controlled by the horizontal motion. The actuators of the slave are remote, in order to allow the grasper to enter a trocar with a 15 mm diameter. Each actuator is mechanically linked to its relative grasper arm thanks to a rod. Strain gauges are implemented to measure the interaction force between the slave grasper and the environment. The position of both master and slave are measured by encoders directly connected to the motor shafts. Both at the slave and at the master side, capstans are used in order to increase the available torque. Obviously, sterilization issues have not been taken into account at this stage of development. By designing and implementing an adequate control law based on the position and force meausrements, it is possible to make the slave reproduce the motion of the master. At the same time, the actuators of the master can reproduce the forces measured at the slave side, making the operator feel the organ. Such control laws have been designed on the basis of models of the master, the slave, the operator and the environement, and tested in simulation. The next step is to implement these control laws on the device, and to test them on a fake lung, or an ex-vivo one.

17

4. Conclusion

The study of lung palpation required to design a haptic interface reproducing the contact with a human lung. To this end, a light weight two degree-of-freedom force sensor able to measure compression and shear forces in significantly different ranges was needed. The sensor described in this paper has a novel elastic frame based on two flexible structures bending around the same axis. The sizing of the structure is based on the study of elementary parts, leading to a straightforward procedure. The elastic frame has been manufactured by electrical discharge machining and equipped with strain gauges. It results in a monolithic, compact and low-cost structure. Thanks to its particular shape, the sensor is linear, and shows high precision and repeatability, low hysteresis and low cross-sensitivity. Additionally, it is versatile and very easy to adapt to specific applications, since its main characteristics (stiffness, sensitivity and bandwidth) only depend on the sizing of a single elementary part.

When the haptic interface is used by an operator to perform a virtual palpation, the force sensor allows to capture a specific force pattern associated with the discovery of a nodule. The detection and amplification of this pattern may make the location of small lesions easier.

Future works will see the implementation of the force sensor, together with an appropriate control law, on a teleoperated palpation device as described in Sect. 3.5.

References

[1] P. Hokayem, Automatica 42 (2006) 2035–2047.

[2] G. Campion, W. Qi, H. V., IEEE Conference On Robotics and Control (2005).

[3] U. Spaelter, D. Chapuis, R. Gassert, M. R., B. H., The First IEEE/RAS-EMBS International Conference on Biomedical Robotics and Biomechatronics (2006) 727 – 732.

[4] A. C. Smith, F. Mobasser, K. Hashtrudi-Zaad, IEEE Transactions On Robotics Vol. 22 (2006) 1163–1175.

[5] M. Tada, S. Sasaki, T. Ogasawara, Proceedings of IEEE Sensors 67 (2002) 984–989.

[6] L. Chen, S. A., IEEE International Conference on Measuring Technology and Mechatronics Automation (2009) 77–80.

[7] G.-S. Ki, The Institute of Control, Automation and Systems Engineers 3 (1) (March 2001) 66–70.

[8] S. Henein, Conception des structures articules guidages flexibles de haute prcision, Ph.D. thesis, Ecole Polytechnique Fdrale de Lausanne, 2000.

[9] M. Nicotra, A. Buttafuoco, M. Kinnaert, To appear in the Proceedings of the 16th IFAC Symposium on System Identification, Brussels (2012).
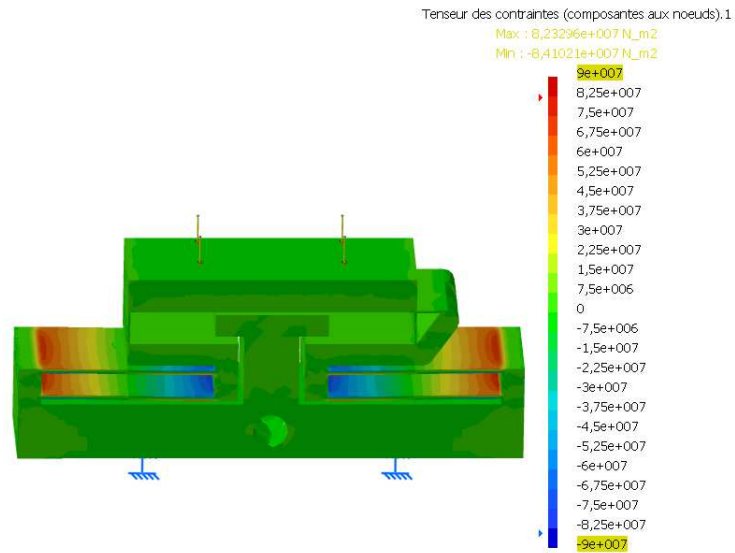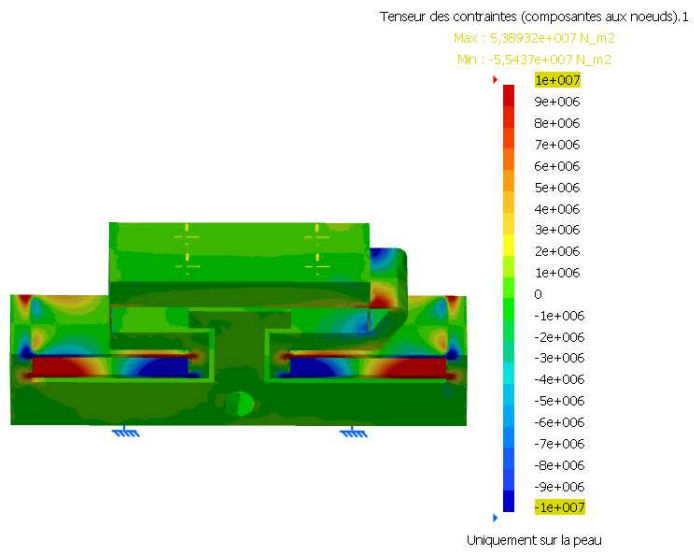
Figure 9: Finite elements analysis of the σ_{xx}component of the stress tensor. On top, bending around the z-axis, due to a $10\,$N force oriented along the y-axis, is considered. On the bottom, the torsion induced by a 100mNm torque around x-axis is considered. The color-scale is expressed in Nm^{-2}.
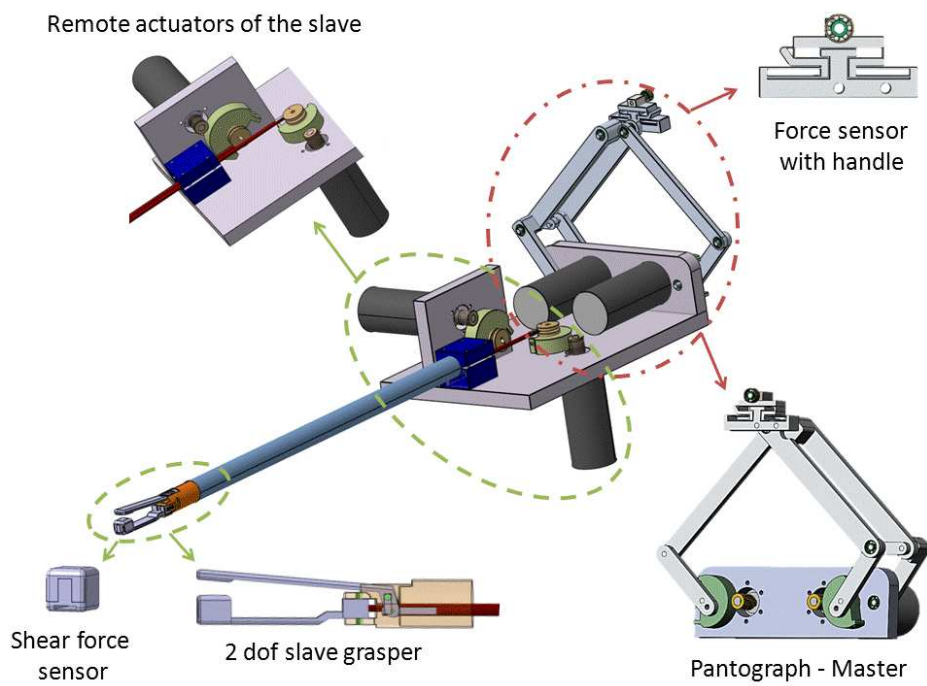
Figure 10: Sketch of the targeted medical tool. The extremity of the 2 dof slave grasper is able to measure compressive and shear forces. The force sensor presented in this work has been developed for the pantograph-master.